The Pennsylvania State University

The Graduate School

Eberly College of Sciences

MECHANISTIC STUDIES IN WATER SPLITTING SYSTEMS

A Thesis in

Chemistry

by

Anne Elizabeth Kaintz

Submitted in Partial Fulfillment
of the Requirements
for the degree of

Master of Science

December 2010

The thesis of Anne Elizabeth Kaintz was reviewed and approved* by the following:

Thomas Mallouk
DuPont Professor of Materials Chemistry and Physics
Thesis Adviser

John B. Asbury
Assistant Professor of Chemistry

David L. Allara
Professor of Polymer Science and Chemistry

Barbara J. Garrison
Shapiro Professor of Chemistry
Head of the Chemistry Department

*Signatures are on file in the Graduate School.

ABSTRACT

In the first of two projects, electrochemical kinetics studies were intended to elucidate the mechanism of hydrogen reduction at a Rh/Cr_2O_3 (core/shell) reduction catalyst for future development in a water splitting system. Ultramicroelectrode (UME) fabrication, including photodeposition and electrodeposition of Rh and Au, and the reliability of the resulting electrodes were explored. It was determined that rhodium does not bind strongly enough to glassy carbon by these photodeposition techniques to allow for its use on rotating disk electrodes. Epoxy deteriorates under conditions of rhodium photodeposition. Niobium is unfit for exposed electrode surfaces because of its many different oxide states. Gold UME surfaces recede with use into their glass insulation surroundings. And 25 μm thick gold and rhodium wires disintegrate in flames too quickly to allow for their use in traditional UME construction.

In the second project, flash-photolysis and time-resolved photolysis studies were intended to illuminate the kinetics of charge transfer for the reduction half of a water splitting system involving hexaniobate nanoscrolls, nanoparticulate Pt reduction catalysts, and $Ru(bpy)_2(4,4'\text{-}(PO_3H_2)_2bpy)^{2+}$ dye. Solid state synthesis and exfoliation techniques were used to produce the nanoscrolls, and XRD and TEM were used to confirm the identity of the product and success of Pt photodeposition.

TABLE OF CONTENTS

LIST OF FIGURES

Chapter 1

Chapter 2

Chapter 3

Chapter 1. Background and Introduction

1.1. Types of Water Splitting Systems

Water splitting using visible light is an attractive form of solar energy conversion, allowing for a clean, renewable source of hydrogen. The most developed method for solar powered water splitting is currently the photovoltaic cell, coupled to an electrolyzer.[1] The problem with this method is that the devices are not simple to make. Because the cost of production would be high, the efficiency requirements would also be high for the devices to be economic. A simpler alternative is to use a particulate semiconductor photocatalyst, which could absorb light, separate charge carriers via a p-n junction, and catalyze the oxidation and reduction reactions on its surface. Recently, several groups[2] have demonstrated overall water splitting with semiconductor particles. These photocatalytic systems are much easier and cheaper to make. Unfortunately, it is difficult to improve semiconductor-based systems because different parts of the charge-separation and catalysis mechanism cannot be isolated for easy study or optimization. A better choice would be a hybrid system, so called because it combines components of semiconductor and molecular photocatalytic systems.

We intend to study the system detailed in Figure 1. Using molecular dyes as sensitizers, instead of semiconductors, allows the absorption wavelengths of the dye to be tuned and its kinetics and mechanism isolated for study. At the same time, it still allows the sensitizer to be adsorbed near the catalytic site, which in principle should lead to less recombination and faster turnover rates (and therefore longer sensitizer lifetimes) than in a purely molecular photochemical system.[1] The use of two different catalysts enables each catalytic pathway to be studied and optimized separately, which could not be done in a semiconductor system. And the solid state catalytic sites allow for all the components of the system to be attached, so that the geometry of the system, and therefore the recombination pathways, can be studied and controlled by modifying the structure as needed.

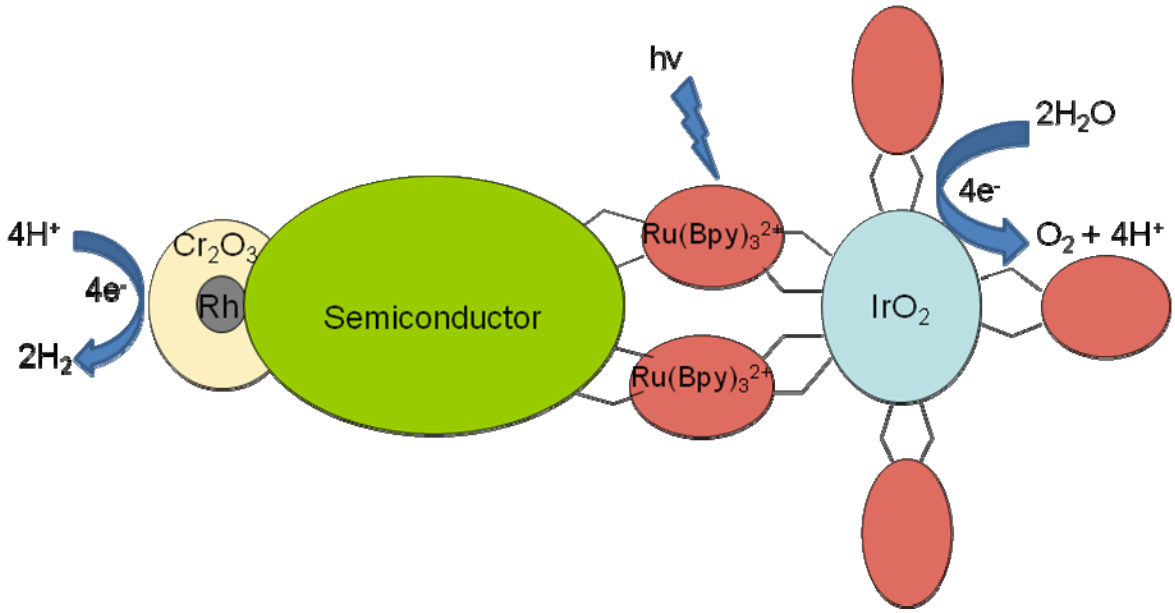

Figure 1. Cartoon of a hybrid water splitting system.

1.2. Choices of System Components

The efficiency of the system is very sensitive to the photoelectrochemical properties of its components (Fig. 2). The sensitizer dye must be sufficiently reducing in the excited state that it can easily inject electrons into the semiconductor. At the same time, after it donates an electron to the semiconductor, the oxidized sensitizer must be sufficiently oxidizing to be rapidly reduced by IrO_2. These factors together dictate the minimum absorption band edge (excitation energy) for the dye. The conduction band of the reducing-side semiconductor must, in turn, be sufficiently negative that it can donate an electron to the catalyst particle, Rh in Fig 1. And both the reduction site and the oxidation site must be at potentials such that they can reduce and oxidize water to form H_2 and O_2, respectively.

$$H_2O \rightarrow H_2 + \tfrac{1}{2}\, O_2 \qquad (E^\circ = 1.229\ V) \qquad (1)$$

The system is further constrained by the requirement that it run under solar excitation. As demonstrated by Bolton, et al, the maximum efficiency for such a system will be found at wavelengths where the absorbed photon flux, related to the solar intensity, is maximized for maximum available Gibbs energy per photon.[3]

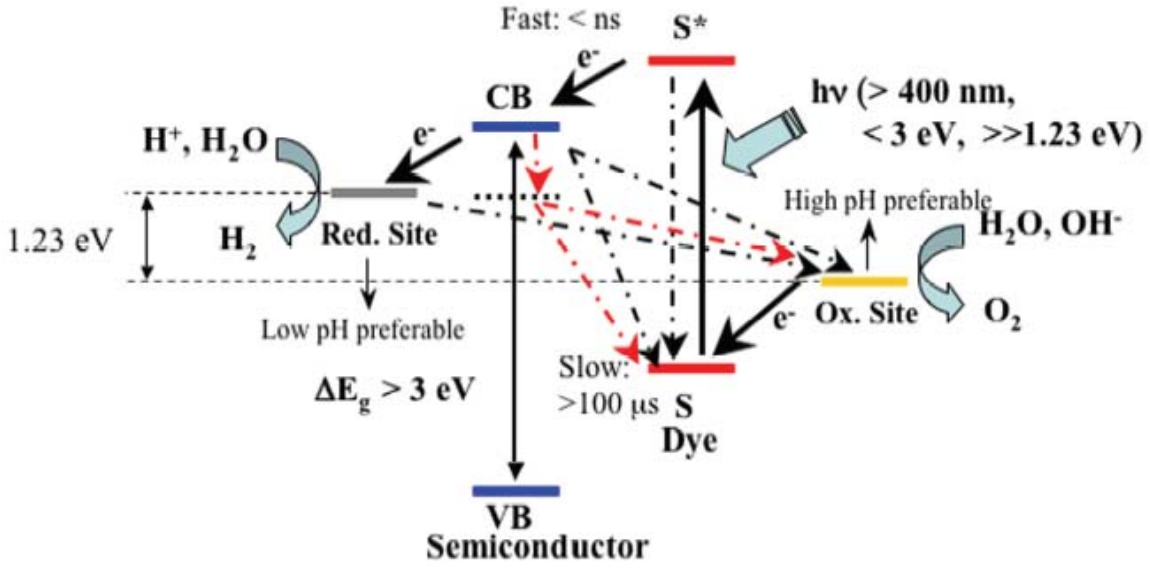

Figure 2. Free energy/redox potential scheme for a sensitizer-semiconductor-catalyst system like that shown in Fig. 1. Solid arrows show the desired forward reactions, and dashed arrows indicate energetically favorable recombination pathways. In reduction half-reaction studies, the oxidation site and oxygen evolution reaction are replaced with the oxidation of EDTA.

Ruthenium polypyridyl dyes (Fig. 3) were chosen for these experiments because of their relation to the oxidation half of the water-splitting system. The most efficient catalyst known to oxidize water to form O_2 under visible light is $IrO_2 \cdot nH_2O$.[4] To minimize charge recombination (Fig. 2) and to increase the lifetime of the dye, it is important that the electron injection rate from the oxidizing catalyst is fast. This is best accomplished by chemically attaching the $IrO_2 \cdot nH_2O$ particles to the dye. The most effective way that has been found to do this is by incorporating the $IrO_2 \cdot nH_2O$ capping groups (malonate or succinate groups) as ligands on the dye and using the dye molecules as capping groups in the $IrO_2 \cdot nH_2O$ nanoparticle preparation. Ruthenium polypyridyl dyes are stable at temperatures well over 100 ˚C and so would weather the conditions of $IrO_2 \cdot nH_2O$ particle synthesis, their absorption edge and electron transfer properties can be adjusted by altering their ligands, and ligand carboxylate groups are particularly easy to attain.[5,6] Phosphonate groups have been found to bind very well to oxide semiconductors, and so were used instead of carboxylates to anchor the dye to the reducing semiconductor. My work on these projects dealt with the reduction half of the water splitting system, but used ruthenium polypyridyl dyes in anticipation of uniting the

two halves. Because the oxidation half was not involved in my studies, my dyes did not have malonate or succinate ligands.

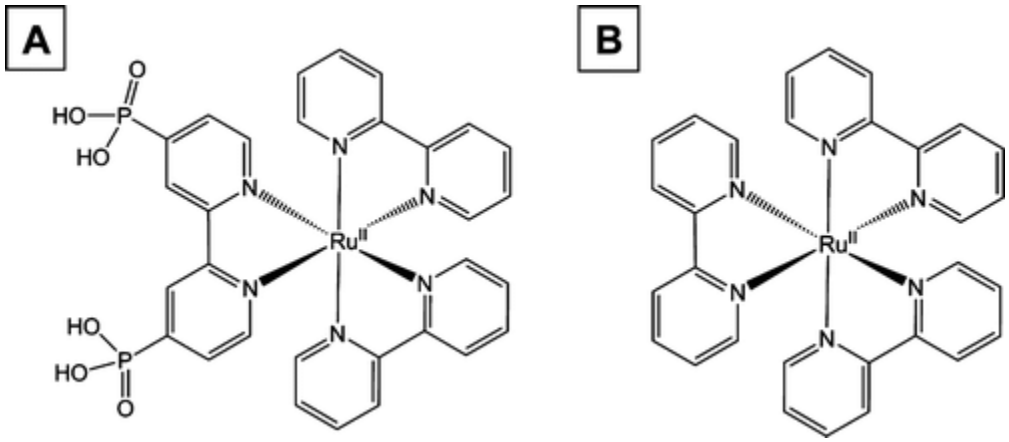

Figure 3. Ruthenium polypyridyl dyes; (a) $Ru(bpy)_2(4,4'\text{-}(PO_3H_2)_2bpy)^{2+}$ and (b) $Ru(bpy)_3^{2+}$. [7]

1.3. Overarching Goals and Strategy

The main goal of these studies was to understand how the mechanisms of charge separation and recombination relate to the spatial structure within the systems. The mechanisms of photo-induced electron transfer between the sensitizer dyes and attached semiconductors have been thoroughly studied and are well understood. Quantum yields for transient charge separation between these components are often quite high, and H_2 or O_2 production with sacrificial donor or acceptor molecules can also be as high as 40 – 70%.[8,9] This suggests that the very low quantum yields found in coupled water splitting systems are due to electron recombination after charge separation had taken place, i.e. the back reaction. The systems discussed in this thesis are ideal for studying these issues. Because the entire system is chemically bonded together, rather than functioning by diffusion of redox pairs, the geometry can be altered to study and minimize the effect of recombination pathways. As the different steps of the mechanism take place in different materials, select pieces of the system can be isolated and studied to allow for determination of the kinetics of the individual steps by a range of techniques, including electrochemistry, and transient diffuse reflectance spectroscopy. This information would then be used to improve upon the efficiency of the system, testing the quantum yield and

rate of H_2 production of the assembled system or half-system by way of time-resolved photolysis.

Chapter 2. Electrochemical Studies of Hydrogen Reduction Catalysts

2.1. Core/Shell Reduction Catalysis in the Literature

The choice of ZnO semiconductor and Rh/Cr_2O_3 cocatalyst for the reduction half reaction was based on several papers by the Domen group detailing a heterogeneous system involving a $(Ga_{1-x}Zn_x)(N_{1-x}O_x)$ photocatalytic semiconductor and Rh-core/Cr_2O_3-shell nanoparticulate cocatalysts. At the time of these experiments, this system had been found to have the highest efficiency of any solid state photocatalysts for solar-light-driven reduction of water to H_2.[10] The use of noble metals as cocatalysts on semiconductors for water reduction aids the charge separation in the semiconductor.[11] This is likely because of the effect of the Schottky barrier creating an internal electrostatic potential barrier. The Cr_2O_3 shell on the Rh cocatalyst was found to greatly reduce the back reaction ($4H_2 + O_2 \rightarrow 2H_2O$), which is also catalyzed by noble metals.[11] Because we used a dye as the sensitizer in our system, we did not need to adjust the semiconductor band gap by adding GaN, and so could use ZnO instead of the $(Ga_{1-x}Zn_x)(N_{1-x}O_x)$ solid solution.

The goal of this project was to study the mechanism of the reduction reaction at the Rh/Cr_2O_3 cocatalyst. At the time, it had been demonstrated by Domen, et al, that systems with Cr_2O_3-coated Rh reduction sites have improved overall water splitting (OWS) over those with bare Rh reduction sites. It was proposed that the Cr_2O_3 shell prevents the back reaction by sealing the Rh off from solution. In this case, the reaction would take place by electron tunneling through approximately 2 nm of oxide to reduce water to hydrogen on the surface of the Cr_2O_3 shell. The back reaction was thought to be eliminated because of the inability of the electrons to tunnel in the opposite direction. This explanation seemed unlikely because Cr_2O_3 is not known to be a good site for hydrogen reduction. It had also been shown that Cr_2O_3 cocatalysits without the noble metal core do not catalyze water reduction,[12] although this could in part be due to the absence of the Schottky barrier. We thought it more likely that the oxide shell blocks the diffusion of O_2 to the surface of the Rh, preventing the back reaction, while allowing the diffusion of H^+ in for the reduction reaction. This mechanism has been found in similar situations with hydrogen evolution on oxide films coating metal electrodes.[13]

2.2. Electrochemical Procedures and Kinetics

Two different types of electrodes were used to try to discover the mechanism of this system. The first, called a Rotating Disk Electrode (RDE), can be rotated at increasing rates in order to increase the mass transport limited current. At sufficiently fast rotation rates, reactants reach the electrode face so quickly that it is the kinetics of the reaction which limits the rate. Under these conditions, the kinetically limited current density, j_k, is much smaller than the mass transfer limited current density, j_l. The second type of electrode, an Ultramicroelectrode (UME) also measures a kinetically-controlled current, although it remains stationary. In this case, the face of the electrode is so small, with a maximum critical dimension of 25 μm, that nonlinear diffusion results in a relatively large j_l, so again for kinetically slow reactions, $j_k << j_l$. Domen's cocatalyst would be approximated by photodeposition of 2 nm Rh particles[14] or electrodeposition of a 2 nm thick pin-hole free Rh film[15,16,17] on an electrode and photodeposition of a 2 nm Cr_2O_3 shell over top of the Rh.[12] The rotation rate or scan rate, for RDE or UME, respectively, could then be varied to find the non-mass-transport-limited current under different temperatures and pHs.[18]

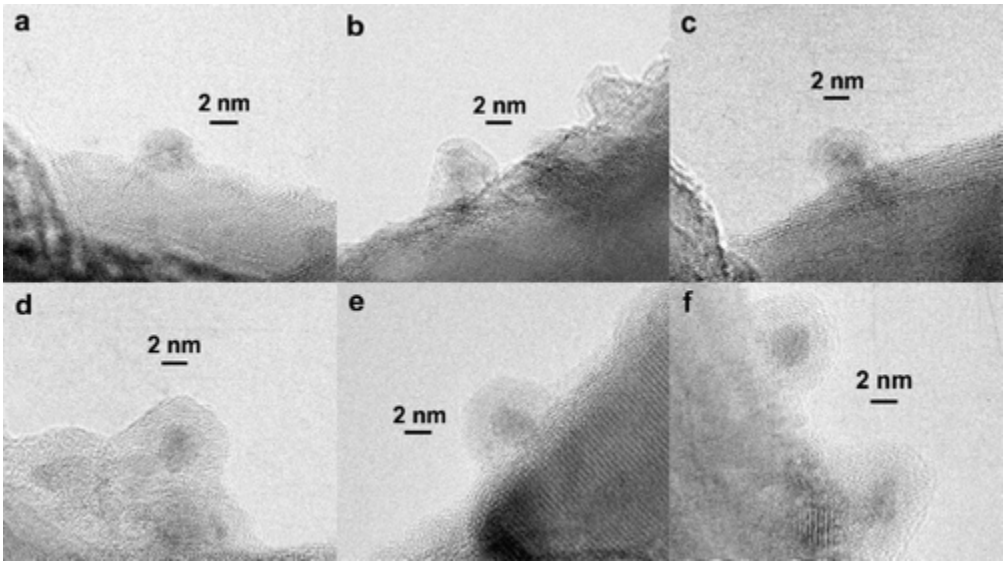

Figure 4: HR-TEM images of Rh-loaded semiconductor (a) before and (b-f) after photodeposition of Cr_2O_3. [19]

Because the resulting current is kinetically controlled, it must be influenced by different variables depending on the mechanism of charge transfer and catalysis.

Because the Cr_2O_3 shells do not show evidence of pin-holes by Transmission Electron Microscopy (TEM) (Fig. 4), a mass transfer controlled current would follow the Koutecky-Levich equation for diffusion to the electrode surface through an inert substrate film (2). The Levich current gives the current where the limiting step is the mass-transport of the reagent A to the surface of the film. In the case where reactant diffusion through the substrate is limiting, the reactant diffusion current will be dominant. When the current is limited by the permeation of A into or out of the film, as opposed to through it, the permeation current dominates the expression.

Koutecky-Levich equation	$1/j_l = 1/j_A + 1/j_S + 1/j_p$	(2)
Levich current	$j_A = 0.62nFC_A^*D_A^{2/3}\nu^{-1/6}\omega^{1/2}$	
Reactant diffusion current	$j_S = nFD_s\kappa C_A^*/L$	
Permeation current	$j_p = nF\chi_f C_A^*$	

In the above equations, F is the faraday constant, C_A^* is the concentration of A in the bulk solution, D_A is the diffusion coefficient of A, ν is the kinematic viscosity, ω is the angular frequency of rotation, D_s is the diffusion coefficient of A in the substrate, κ is the partitioning coefficient ([A] just inside the film/[A] just outside), L is the film thickness, and χ_f is the rate constant for the transport of A into the film. The current density j is the current (i) divided by the electrode area. For a given type and thickness of substrate, reactant A, and electrolyte, it is clear that the diffusion-controlled current will be dependent on the concentration of A in the bulk solution and on temperature, to the degree that diffusion coefficients are dependent on temperature.[18]

As 2 nm is a relatively large distance to tunnel across, if tunneling is involved in the mechanism it is likely to be the rate-determining step. Tunneling rates in this system would be dictated by the Fowler-Nordheim equation (3).

Fowler-Nordheim equation	$R = \exp[-4(2m)^{1/2}\Phi^{3/2}/(3\hbar eE)]$	(3)
where $\Phi = \Phi_o - k_\beta T$ and $E = \Delta V/L$ to give R proportional to $-(\Phi_o - k_\beta T)^{3/2}L$		

In the above, Φ_o is the work function under standard conditions, T is the temperature, L is the thickness of the insulating oxide shell, and m, $\hbar$, e, and k_β are constants. Clearly, a tunneling-controlled current would not be proportional to reactant concentration but would vary exponentially with the thickness of the film and, to some small degree, would depend on temperature. Determination of the dependence of the non-mass-transport-

limited current on different pH, temperature, and film thickness would clarify which of these mechanisms is followed. If it were found that H^+ diffuses through the shell, fitting the data to the appropriate variation of the Koutecky-Levich equation would show more specifics of the diffusion mechanism.[18] Substituting Rh with a metal that is not catalytic for hydrogen reduction could verify the results of these experiments as diminished hydrogen reduction rates would support a diffusion mechanism, while rates similar to those found with Rh would support a tunneling mechanism.

2.3 Preliminary Measurement of Water Redox

Before beginning kinetics experiments, some reactions were run to demonstrate the proper use of the system by producing known data with regard to the reduction of water at an RDE. An unexpected cathodic limiting current was found where the hydrogen evolution current was expected on both the Pt and Rh electrodeposited electrodes in the range of 2.5 to 6.5 pH. According to the Nernst equation, in a solution of 3.16E-5 M H^+ (pH 4.5) and 7.9E-4 M H_2 (solubility at 1 atm), the reduction potential for hydrogen evolution should be -0.416 V vs. SCE. The current was mass-transport limited, eliminating the possible explanation of an oxide film. It was also present with both Na2SO4 and NaClO4 supporting electrolytes regardless of their concentration, eliminating both the possibility contaminants in the supporting electrolyte and the possibility of SO_3^{2-} blocking hydrogen reduction at the electrode.[20] Eventually, it was found that the limiting current was due to the mass-transport-limited reduction of hydronium ion at more positive potential. The reduction of water to form molecular hydrogen happens at a more negative potential and is, of course, not mass-transport limited in aqueous solution.[21,22,23,24]

The reliability of the experimental procedure was shown by measuring the limiting current for the reduction half-reaction vs. the charging current at different pHs. These values were shown to have a linear relation to the concentration of hydronium ion in solution. In kinetics experiments, reaction potentials would be calculated from similar experimental procedures via a Tafel plot.

2.4. Rhodium Deactivation on Glassy Carbon RDEs

To acquire kinetics data for bare rhodium, before moving on to the oxide-coated surface, Rh was electrodeposited onto a glassy carbon RDE.[15,16] Glassy carbon was chosen as an ideal material for this purpose because it does not catalyze the reduction of water to hydrogen, unlike rhodium. The reaction on Rh would therefore be an inner-sphere reaction whereas it would be outer-sphere on glassy carbon. As rhodium provides the more kinetically favorable site for the reaction, and therefore the lower reaction potential, the reaction could be assumed to only take place on the surface of the rhodium. Had an electrode made of another noble metal, such as platinum or gold, been used, it would have had to have been coated with a pin-hole-free layer of rhodium in order to assure that the reduction of water would happen only at rhodium interfaces. Once the deposition was completed, it was found that the oxidation limiting current decreased with each sweep, although the reduction current did not. (Fig 5)

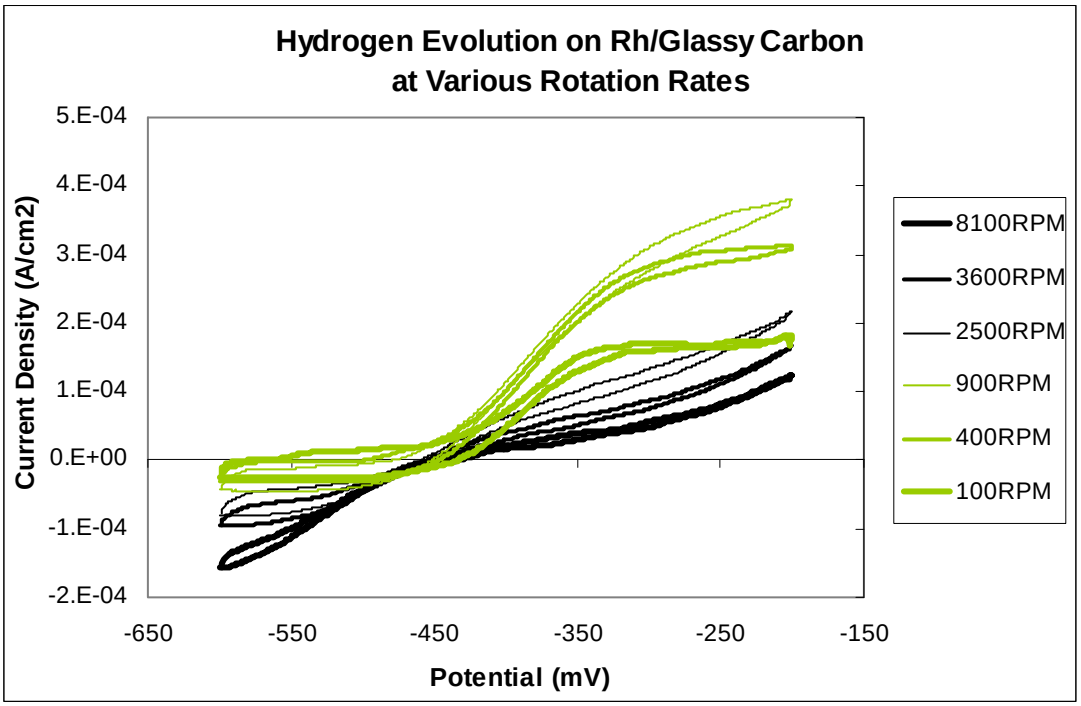

Figure 5. Zero-current potential in 4.5 pH H_2SO_4, 0.1 M Na_2SO_4, and 1 atm H_2 at 1600 RPM and 10 mV/s.

This could be explained if something was happening to the Rh surface which effectively lessened the electroactive surface area of the electrode with time. The kinetically-limited current would be smaller with a smaller active surface area. Beyond a

certain degree of Rh deactivation, the anodic kinetically-limited current would be unable to keep up with the mass-transport-limited current, causing the current to drop off as ever more Rh was deactivated. Apparently, the cathodic kinetically-limited current was not smaller than the cathodic mass-transport-limited current for the same amount of active Rh, because of the interaction of the rate constants and reactant concentrations. It is unlikely that the rhodium was being oxidized, as the experimental conditions were well within the stable Rh region of the relevant potential-pH equilibrium diagram (Fig. 6).[25]

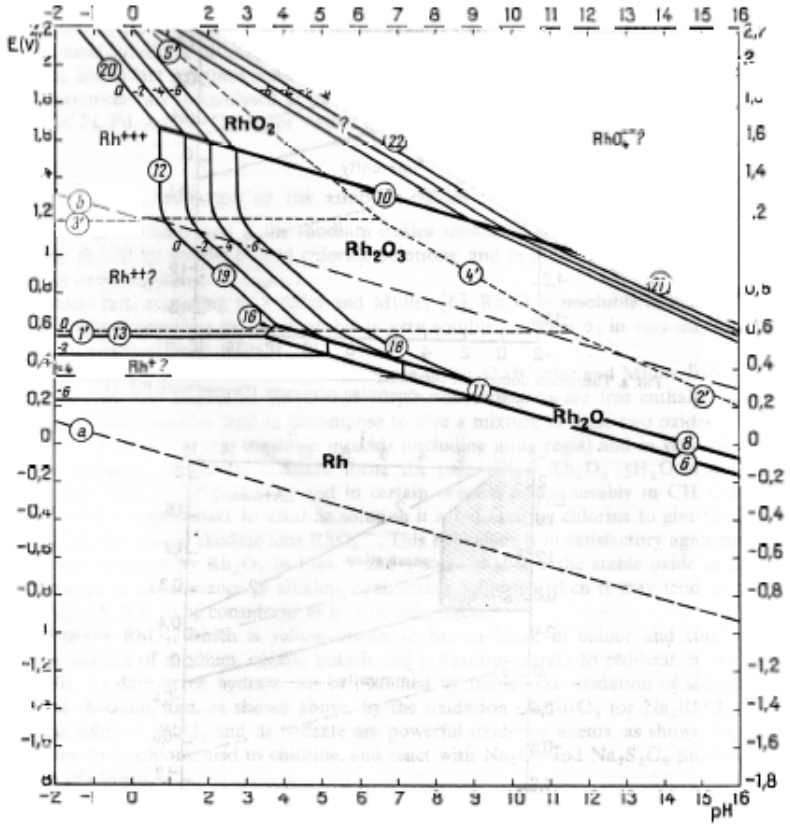

Figure 6. Potential-pH equilibrium diagram for a rhodium-water system at 25 ℃.[25]

Decreasing the range of potential scanned did not eliminate this effect, as had been hoped, by eliminating the opportunity for poisoning of the Rh at more extreme potentials. When the cyclic voltammogram was taken again, then the RDE was rotated at high speed and open circuit, and the cyclic voltammogram was repeated, the same deterioration of the anodic limiting current was observed. Apparently, the loss of catalytic surface area is due to removal of the Rh by agitation from the rotation of the electrode (Fig. 7). Although it would have been unlikely that such agitation could dislodge a 2 nm thick layer of Rh,[15] it is probable that in my experiment, particles were

formed. Yan deposited Rh on a gold film whereas I deposited directly onto glassy carbon. Rh on Au follows a Stransky-Krastanov mechanism of layer-by-layer growth while Rh on glassy carbon follows a Volmer-Weber mechanism, in which it is more energetically favorable for Rh to bind to Rh than for it to wet the carbon surface.[17]

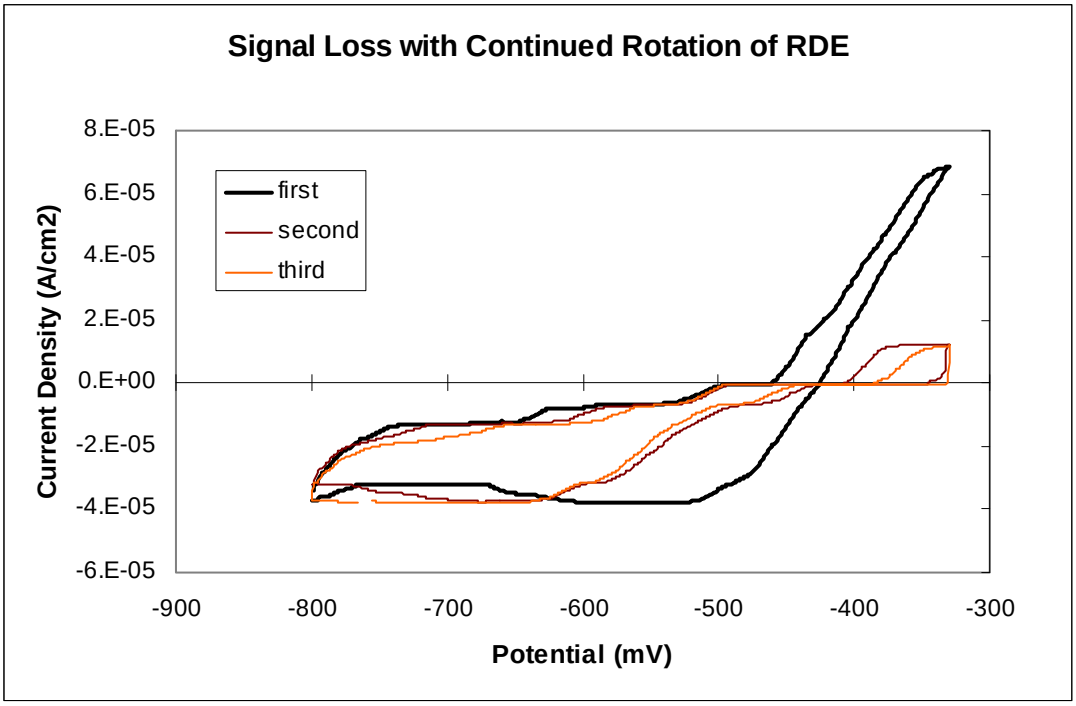

Figure 7: Rh dislodged by agitation with rotation over time. The first scan is with a fresh deposition, the second after 30 min at 3600 RPM, the third after 60 min at 3600 RPM. Each measurement is of hydrogen redox at 100 RPM in 4.57 pH solution at 5 mV/s scan rate with a hydrogen purge.

2.5. Construction and Testing of Niobium Ultramicroelectrodes (UMEs)

2.5.1 Epoxy-Sealed Niobium Band UMEs

Because deposition of rhodium onto glassy carbon seemed unlikely to result in Rh which was strongly-enough adsorbed to withstand high numbers of rotations per minute (RPM), rhodium was instead deposited onto homemade niobium band UMEs. A cross-section of niobium foil formed the face of these electrodes, which was electrochemically connected to a copper wire with silver epoxy. A non-conducting adhesive was used as the insulator. In initial experiments, $Rh(OH)_3$ was photodeposited onto 0.00025 cm^2 niobium band UMEs from a 20 mL solution of $5.47x10^{-5}$ M $RhCl_{3(aq)}$, excess TBAOH, and 10% methanol, by volume. Lower concentrations of $RhCl_3$ did not yield signal when

the resulting electrode was reduced and used as the working electrode in an electrolyte of 4.5 pH $H_2SO_{4(aq)}$, 0.1 M $Na_2SO_{4(aq)}$, purged with H_2. This signal (Fig. 8), taken at a scan rate of 3 mV/s for steady state data, was found to be non-Nernstian and irreversible or quasi-reversible. It also exhibits relatively large overpotentials.

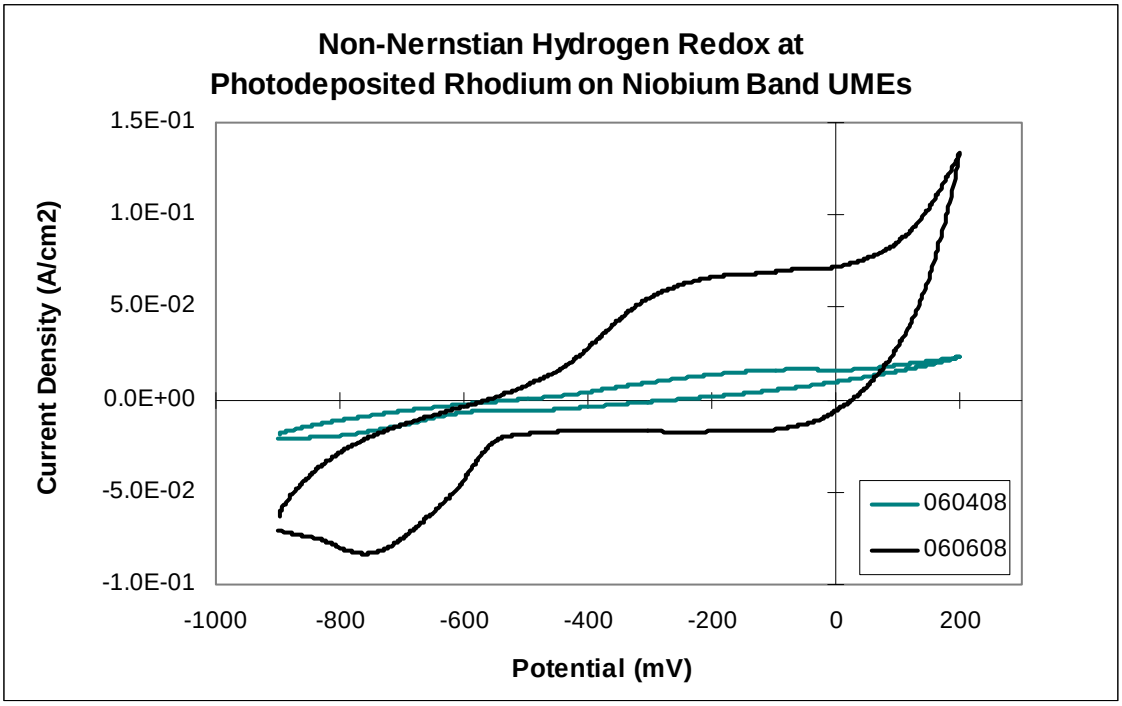

Figure 8: Hydrogen reduction and oxidation using a Rh deposited Nb band UME on two different days in 4.5 pH H_2SO_4, 0.1 M Na_2SO_4, 1 atm H_2 purge.

By contrast, steady state at a Pt RDE in the same solution gave the signal shown in (Fig 9). It was expected that since Pt and Rh both catalyze the hydrogen reduction reaction in aqueous solutions, the Rh/Nb electrode would yield a signal similar to that of Pt, but this is clearly not the case.

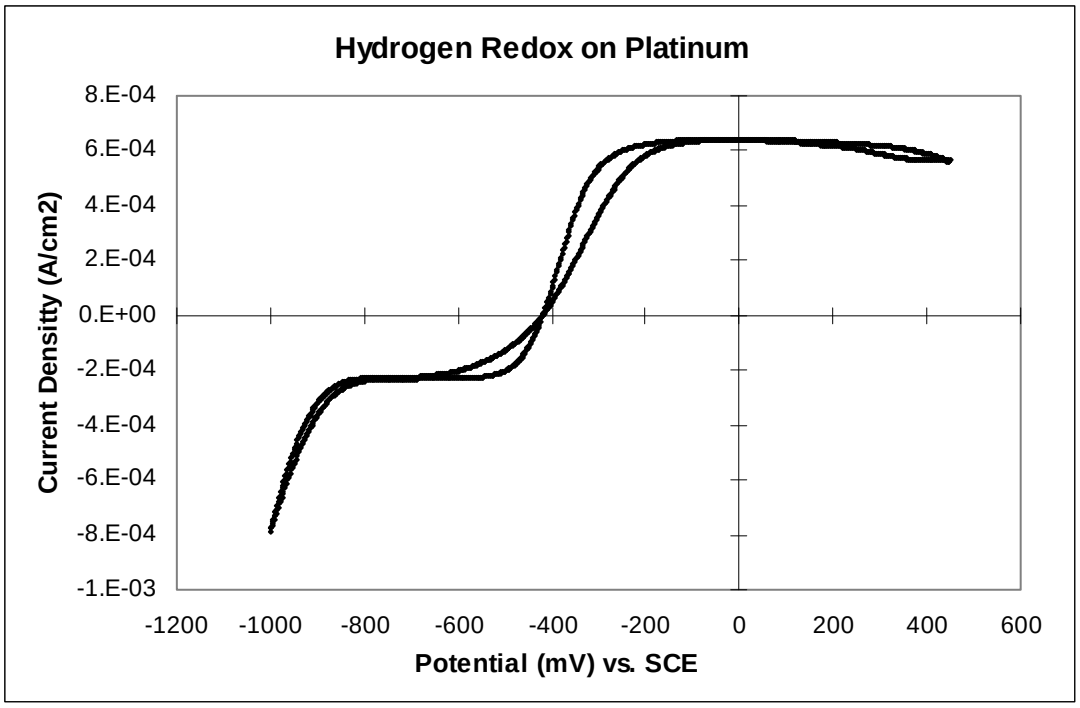

Figure 9. Hydrogen reduction and oxidation on a platinum RDE (0.78 cm^2) at 1600 RPM, 10 mV/s scan rate, 4.5 pH H_2SO_4, 0.1 M Na_2SO_4, under H_2 purge.

In order to diagnose the cause of this surprising data, the UMEs were tested, using a simple, organic, one-electron redox couple. 1,1'-dimethyl-4,4'-bipyridinium hexafluorophosphate (methyl viologen) (1 mM) was chosen as the analyte for the one-electron redox system, with 0.1 M tetrabutylammonium tetrafluoroborate ($TBABF_4$) as the supporting electrolyte in acetonitrile, which was purged with argon. This system was chosen because it avoids any water redox chemistry, methyl viologen is very well studied, and the reduction of methyl viologen should not involve electrode surface chemistry and so could be conducted on the unmodified Nb surface, without Rh deposition. Cathodic peak current potentials for this electrolyte were found at -531 mV and -929 mV vs. SCE using a reliable 0.78 cm^2 platinum disk electrode with a Pt wire counter electrode. This data did not at all match that which was found using a Nb band UME working electrode (Fig 10). Although the cathodic sweep does exhibit a limiting current around -900 mV, approximately the same potential as the second reduction peak on Pt, this is the only clear cathodic wave in the data. The return sweep does not in any way retrace this limiting current. The other plateau region around -500 mV, roughly the

same potential as the first reduction peak on Pt, has a current of about 1.4×10^{-5} A/cm^2, close enough to zero to be merely charging current.

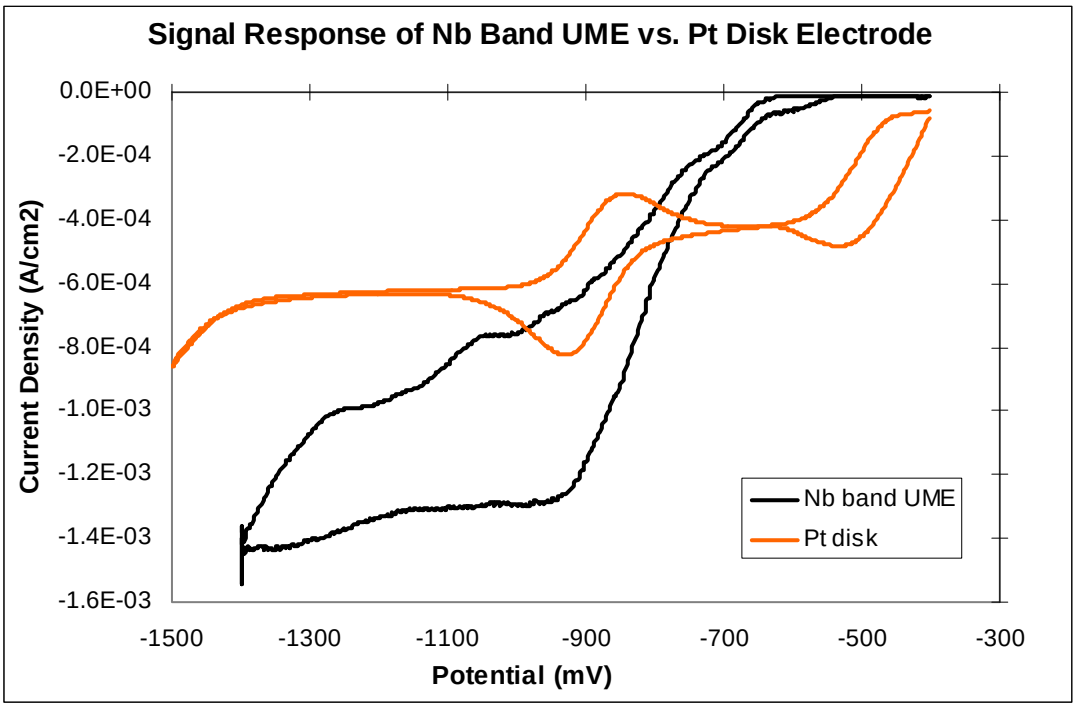

Figure 10: Reduction and oxidation of methyl viologen (1 mM) at 10 mV/s scan rate in 0.1 M TBABF4 under Ar purge. The Pt disk electrode was not rotated, but its signal was magnified by 10 times for easier comparison.

It seemed possible that the epoxy used to seal the face of the band UMEs may have reacted with the Rh photodeposition solution, partially disintegrating the epoxy which could result in leaks and contamination of the electrolytes. No odor was noticed upon opening scintillation vials after deposition onto bare Nb foil, but a foul smell was apparent when opening a scintillation vial after deposition onto the Nb band UMEs, which were sealed with epoxy. Furthermore, the epoxy on one of the Nb band UMEs disintegrated so much after only two photodepositions and four separate days of electrochemical experiments that the epoxy detached from the glass tube, allowing the tube to fill halfway with reaction solution. A small applied force freed the face of the electrode from the glass tube and copper wire contact, demonstrating that the conducting silver epoxy used to make the electrical contact had also deteriorated. Although Rh nanoparticles were not present on faces of the electrodes during electrolysis of methyl viologen, the same electrodes had been used previously with Rh deposition. This idea that deterioration of the epoxy was the cause of the strange signals was tested by making

some Nb disk UMEs. These made electrical contact by solder and were sealed with glass and were therefore free of epoxy.

The construction of the disk UME also addressed another potential problem of the band UMEs. Although the critical dimension of the Nb band electrodes was small enough (25 μm) that they should have behaved as UMEs, semi-infinite linear diffusion, was still observed when the band UMEs were run in aqueous solutions (Fig 8). It seemed likely that this was due to the difficulty in polishing the Nb band UMEs. Because it took a significant amount of time to polish the Nb smooth after sanding, and because the epoxy is so much softer than the Nb, the epoxy often wore away much more quickly than the Nb, causing the Nb foil to protrude from the epoxy so much so that it could sometimes be seen by the unaided eye. This likely resulted in a critical dimension greater than 25 μm, one which varied with each new polishing of an electrode. Because the hardness of niobium is much closer to that of glass than epoxy, this was not a problem with the Nb disk UMEs, which were sealed with glass rather than epoxy, and the electrode face did not protrude much, if at all, after polishing.

2.5.2. Glass-Sealed Niobium Disk UMEs

Construction of the Nb disk UMEs was surprisingly difficult. Most solders don't work on Nb because they cannot adhere to the oxide layer, and unlike many other metals, niobium cannot be prepared for soldering by removing the oxide immediately beforehand because the oxide layer re-forms too quickly. According to U.S. Patent 5592732, lead-indium solder would work with Nb.[26] The lead was assumed to be present in the solder purely to accommodate superconductivity, as this was a major focus of the patent, and indium ingots were used as solder, instead. This resulted in firmly held wires and good ohmic contact. Sealing the 25 μm thick Nb wire in a glass capillary was also very difficult, as the glass did not easily wet the Nb and holding the glass-sheathed Nb in the flame for too long often oxidized the wire so much that it disintegrated. The best method found for making the Nb disk UMEs was to first make and test the electrical contact, and then insert the soldered wires into the glass capillary for heat sealing. The face of the glass-enclosed Nb was sanded and polished flat afterwards.

2.5.3. Niobium as an Electrode Surface

As can be seen in Figure 11, use of a niobium disk UME did not fully address the problems with the niobium working electrode data. In order to determine whether the inconsistencies between the Pt and Nb electrode signals is the result of faulty electrodes or some effect of the Nb surface, Nb foil on the scale of 0.25 cm^2 to 0.5 cm^2 was used as a working electrode in the methyl viologen electrolyte (Fig. 11). The Nb band UME and the Nb foil give strikingly similar wave shapes, suggesting that the structure of the UMEs is not the cause of the messy data. The difference in current density can be attributed to the substantial difference in size of the two working electrodes.

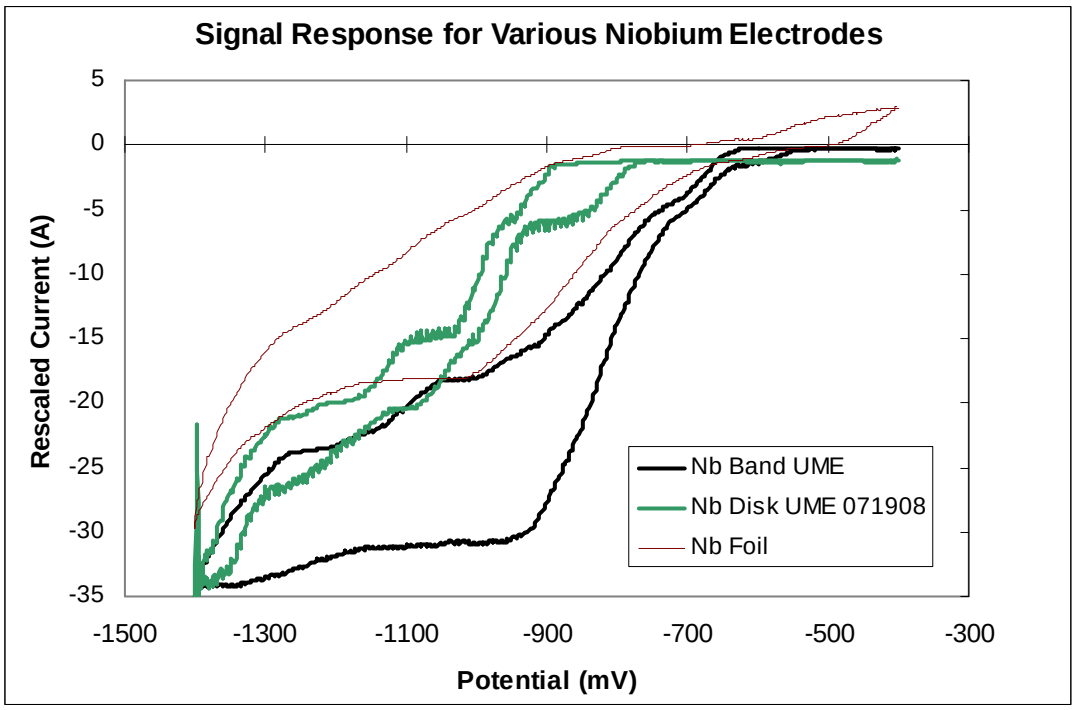

Figure 11. Methyl viologen (1 mM) redox at 10 mV/s scan rate, in 0.1 M TBABF4, under 1 atm Ar. The volatmmograms from the different electrodes were rescaled for easy comparison.

Perhaps most convincingly, one of the Nb band UMEs was coated with an approximately 10 nm thick Pt film and used as the working electrode in the methyl viologen system. Sputtering was found to be the best available technique for application of the film. According to Mikhailova, et al, electrodeposition of Pt onto an Nb electrode is impractical because too thin a niobium oxide layer allows hydrogen adsorption on the niobium oxide from the aqueous Pt plating solution which, with HER, causes exfoliation

of the Pt layer. Too thick a layer of oxide results in crumbling of the oxide which also prevents the platinization. These authors found only a very specific preparation of the Nb surface, involving mechanical abrasion of the surface, HF etching, and a very precise and undisclosed thermal treatment of the unoxidized Nb surface, would allow electrodeposition of Pt onto Nb.[27] It was also decided that deposition of Pt by a H_2PtCl_6 dip followed by heating would be impractical because the 400 °C bake might destroy the epoxy seal around the UME face, costing a couple days of preparation. There were only two differences between the sputtered Nb band UME and the other Nb band UMEs. First; the face of this electrode points perpendicular to the length of the electrode whereas the others do not. This was done to allow it to fit in the sputtering chamber. Secondly; due to difficulty with masking, the Pt was sputtered over a larger area than just the Nb band and this electrode was therefore not a UME.

The cyclic voltammograms obtained using the platinized Nb band UME are very similar to those obtained using the 0.78 cm^2 diameter Pt disk (Fig. 12), although after the platinum was removed, the UME gave data which was similar to all the other Nb band UMEs. This also suggests that the inconsistencies between data obtained with the Pt and Nb electrodes in methyl viologen are the result of differences between the two metals.

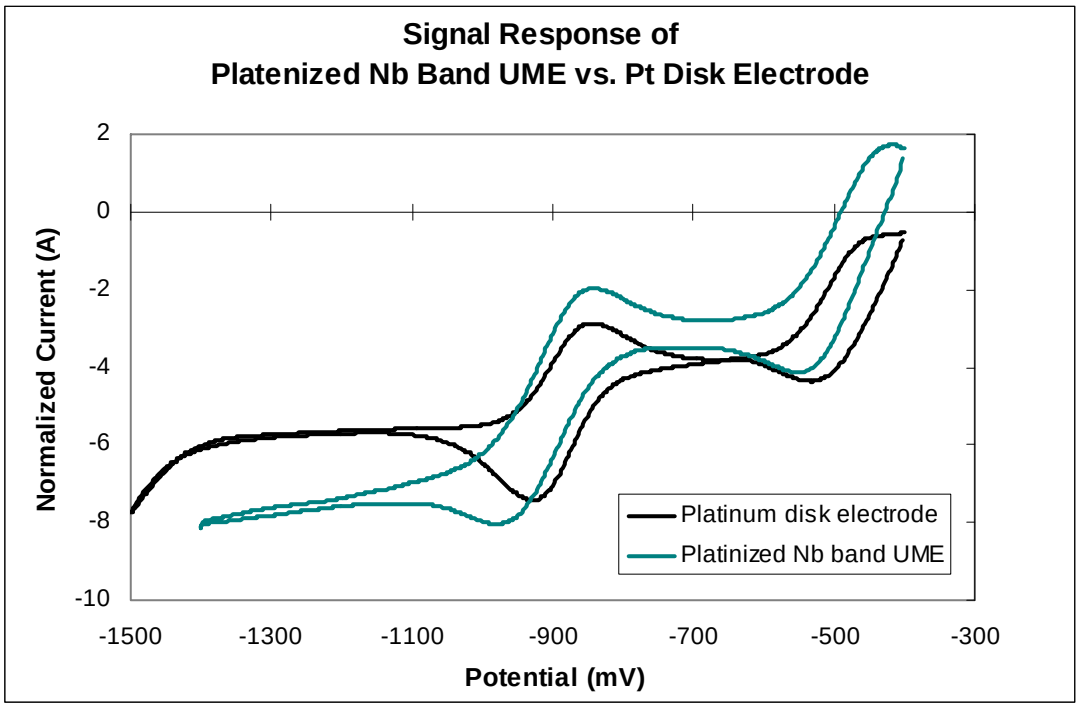

Figure 12. Methyl viologen (1 mM) redox in 0.1 M TBABF4, under 1 atm Ar. The niobium band UME was platenized by sputtering, resulting in a larger Pt electrode face.

2.5.4. Photoreduction Time for Rhodium Deposits on Niobium

An experiment was run in an effort to determine whether the surprising behavior of photodeposited Rh/Nb band UMEs was due to incomplete reduction of the deposited $Rh(OH)_3$ to Rh prior to electrochemical hydrogen evolution experiments. In general, the electrodes were held at -2 V vs. SCE for approximately 5 minutes in the pH 4.5 $H_2SO_{4(aq)}$ electrolyte to reduce the $Rh(OH)_3$ to metallic Rh. In this experiment (Fig 13), cyclic voltammograms of the HER followed longer and longer amounts of time for which the same photodeposited UME was held at -2 V vs. SCE. This experiment was run using a UME which had given signal two days prior and been unaltered since. As can be seen, although the current density increased with increasingly long exposure to negative potential, the signal did not increase proportionately. The increase in current is likely the result of hydrogen permeation of the niobium oxide layer (Nb_2O_5). According to Vaskevich, et al, hydrogen permeates into Nb_2O_5 when Nb electrodes are held at potentials negative of -400 mV vs. SCE and eventually causes a transition of the oxide from semiconducting to metallic behavior.[28] It is clear that one of two things was happening as reduction of the UME continued. Either hydrogen permeated the niobium oxide layer, causing the charging current across the water/metallic $H_xNb_2O_5$ interface to dwarf the HER signal from the Rh catalysts, or the Rh was removed or poisoned with time while the charging current increased.

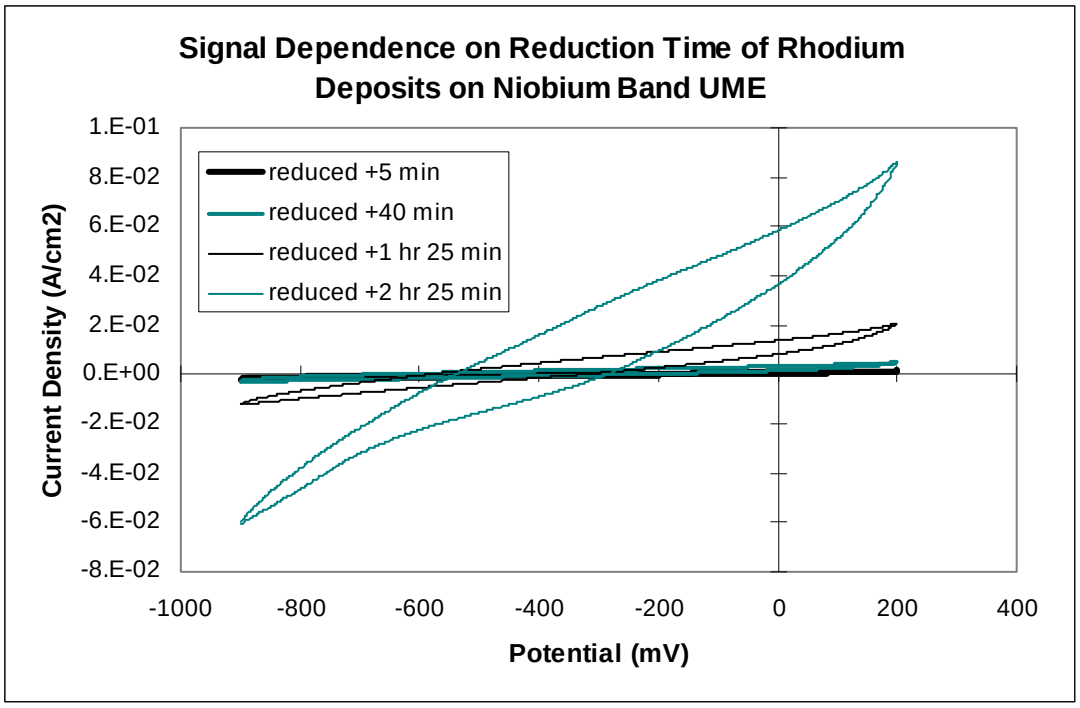

Figure 13: Voltammograms following increasing periods of time during which the electrode was held a -2 V vs. SCE. Measurements were taken with 10 mV/s scan rate, 4.5 pH H_2SO_4, 0.1 M Na_2SO_4, and a H_2 purge.

Whether the poor electrochemical data yielded by the niobium electrodes was due to metallic behavior of the hydrogen-permeated oxide film, or simply to unwanted transitions between the many different oxide states of niobium, it became clear that niobium would not work as an exposed electrode face. The similarity of data found with the platinum-sputtered Nb band UME to data found with a Pt disk electrode suggested the possibility that niobium electrodes would work if covered with a pin-hole free layer of Rh, but sputtering would not be an option for such deposition, since it could not ensure a small enough electrode face for UME behavior. As electrodeposition of Rh onto the niobate would likely suffer from the same problems as electrodeposition of Pt onto niobate,[27] niobium electrodes were abandoned in favor of gold.

2.6. Construction and Testing of Gold UMEs

2.6.1. Rhodium Deposition on Glass-Sealed Gold UMEs

Rhodium was electrodeposited onto a 25 μm diameter gold UME by plating at a cathodic current of 100 μA for 100 s in a $5x10^{-3}$ M $RhCl_3$, 0.1 M $HClO_4$ M electrolyte. This was expected to give a 2 nm thick, pin-hole free layer of Rh. In the literature, the

presence of Rh was affirmed electrochemically by the adsorption of CO on Rh. The absence of pin-holes had been electrochemically verified by demonstrating the absence of CO adsorption on Au and of a gold oxidation peak.[15] Because of the toxicity of CO, O_2 was used instead. Molecular oxygen also adsorbs highly on gold and its oxidation and reduction peaks on Au and Rh are non-overlapping.[29] Electrochemical pretreatment for gold electrodes was taken from Fernanda.[30] Several attempts were made, using deposition times as long as 1000 s, but no peaks for oxygen adsorption on rhodium were found. Some of the samples showed oxidation of gold and some did not. A different rhodium deposition method was tried instead, one which did not claim to deposit a pin-hole free layer, but which had been found to deposit larger amounts of rhodium.[31] This deposition method showed no gold oxidation, but also showed no oxygen adsorption on rhodium.

In order to determine whether rhodium was being deposited, the electrode was analyzed by Energy-Dispersive X-Ray Spectroscopy (EDS). Rhodium was not detected by EDS on the face of the Au UME. This would have indicated that the Rh depositions had failed except that some of the intense gold lines were also missing while others were present. As it was the intense Au lines with longer wavelength which were missing, while those with shorter wavelength were present, it was determined that the face of the UME was depressed below the surface of the surrounding glass. Because the EDS detector is offset from the electron beam by 40º, the signal scattering off a deeply inset surface would have to travel through the surrounding glass in order to reach the detector. Only a 10 nm thick layer of Rh was expected, given the deposition on the electrode which was imaged, making up about 5% of the analysis volume of the sample for EDS. The path length through the glass was apparently enough to absorb Au lines which would otherwise have been visible, suggesting that the much less intense Rh signal would never be detected from this electrode. The depression of the electrode face was confirmed by optical microscopy, by focusing on first the glass at the tip of the electrode, then focusing on the electrode face and noting the height of each, provided by the software. Unfortunately, the exact difference could not be calculated by this method, because the electrode face was so small that the surrounding glass blurred over the face of the

depressed electrode when attempting to bring it into focus. The depression was a minimum of 5.4 μm deep.

A new Au UME of the same variety was purchased to address this problem, Rh was deposited by the same method and the deposition was again checked for completeness via oxygen adsorption and reduction/oxidation of exposed gold. After several unsuccessful attempts at pin-hole free rhodium deposition, it was found by optical microscopy that the surface of the Au UME had receded approximately 3 μm below the glass tip of the electrode, although the electrode was only ever cleaned with polishing cloths and alumina polish. Furthermore, the glass immediately surrounding the gold face of the electrode appeared to have deteriorated over the course of three days of use.

2.6.2. Plastic-Sealed Gold UMEs

To avoid the problems encountered with the glass-encased Au UMEs, I instead decided to construct a gold disk UME. This method of construction differed considerably from that involving 25 μm thick Nb wire sealed in glass capillary tubes. In this construction method, 25 μm thick Au wire was sealed in the tip of a disposable glass or plastic pipette using epoxy, which was sanded flat and polished after thorough drying. Electrical contact was made between the Au wire and a much thicker Cu wire with a small quantity of Hg which was sealed into the pipette, along with the Cu wire, by closing the top of the pipette with epoxy as well. The problem encountered earlier with the protrusion of the electrode face from the surrounding epoxy was expected not to be a problem in this case because Au is so much softer than Nb that it would be polished away faster that the epoxy would, causing a slight divet rather than a protrusion, the surface area of which could be measured by electrochemical means. A pretreatment method for the Au UME and a method for measuring the surface area were found in the literature.[32] Unfortunately, when attempting to measure their surface area in $5x10^{-4}$ M ferrocenemethanol with a sodium sulfate supporting electrolyte, these UMEs did not give a consistent voltammogram. It was considered that the fine 25 μm thick Au wires might have been snapping off because they were so weak, and therefore unable to make good electrical contact. To test this, similar electrodes were made using 25 μm thick Pt wire, which would have been more resilient than the Au while still allowing similar

mechanisms of rhodium deposition. These electrodes gave similarly unreliable data. At this point, this project was abandoned in favor of another.

Chapter 3. Photolysis Studies of Hexaniobate Nanoscrolls in Photocatalytic Hydrogen Evolution

3.1. Layered Metal Oxide Semiconductors (LMOSs) in the Literature

Our group has found in the past that photoinduced hydrogen production from water and non-sacrificial donors is possible with layered metal oxide semiconductors (LMOS's) using visible light. Nanoparticulate platinum was selectively deposited on only the inner layers of the $K_2H_2Nb_6O_{17}$ LMOS, which was sensitized with ruthenium-tris(2,2'-bipyridyl) dye. In this system, molecular hydrogen could be formed from HI in a non-sacrificial reaction because the triiodide could not intercalate the negatively-charged LMOS to reach the Pt catalytic sites.[33] The rate of electron injection from the sensitizer into the semiconductor is three orders of magnitude larger than the rate of back electron transfer from the semiconductor to the triiodide. Despite this, charge recombination is still an issue in this system, because electron migration from the injection site to the reduction site is slowed by the low rates of interlayer conductivity, leaving plenty of time for back electron transfer. Interlayer spacing, determined by ion exchange of the cation from the iodide salt with potassium and hydrogen from the LMOS, was found to be directly correlated to the rates of molecular hydrogen evolution.[34,35]

The slow electron migration through the LMOS to the catalytic site could be addressed by replacing the LMOS $K_4Nb_6O_{17}$ nanoparticles with single crystal $H_4Nb_6O_{17}$ nanoscrolls. Because the hexaniobate nanoscrolls are single-crystalline, electrons may not tunnel in order to move between the different layers, but instead move through the crystal lattice in the plane of the sheets.[34,36] Nanoscrolls and LMOS's hold appeal for water splitting systems not only because of their ability to isolate the reduction catalysts from oxidized species in solution, but also because of the geometric arrangements they make possible. Both the semiconductor particles and the oxidation catalyst particles are far larger than the sensitizer molecules. This poses the problem of how to have more than just a few of the sensitizer molecules in contact with many of the opposite type of particle. One possible solution to this problem is to coat the oxidation catalysts with sensitizer capping ligands and then wrap or layer the scrolls or LMOS's, respectively,

around the oxidizer particles. This type of an arrangement would allow maximum usage of the sensitizer particles, but would present a problem with respect to the compartmentalization of the reduction catalyst, which would no longer be isolated from the oxidized species in solution by its intercalation. This problem could be addressed by the Rh-Cr_2O_3 core-shell arrangement explored by Domen, et al.

Kazuhiko Maeda explored several different layered materials as well as $K_4Nb_6O_{17}$ nanoscrolls as semiconductors in the production of hydrogen from water with nanoparticulate noble-metal catalysts and EDTA as a sacrificial donor. He was able to maximize the quantum yield for molecular hydrogen evolution for various solution pH, dye loadings, and weight percent loadings of a Pt reduction catalyst.[36] All of this work was done by steady-state photolysis. Although it succeeded in determining the relative rates of charge separation and recombination in the system, no absolute rates or rate constants were measured. In order to proceed with this work, it would be necessary to obtain more precise kinetic data about the system. If rate constants were known for the various forward- and back-electron-transfer steps, quantum yields could be improved by altering the system in order to slow the recombination steps or facilitate the forward rate-limiting steps. The kinetics could be determined by way of diffuse reflectance flash-photolysis spectroscopy. A diffuse reflectance system would be necessary because the size of the nanoscrolls is such that the light scattering renders transmission mode flash-photolysis impossible.

3.2. Synthesis and Preparation of Hexaniobate Nanoscrolls

The layered $K_4Nb_6O_{17}$ niobate was produced by grinding together K_2CO_3 (2.2 mol) and Nb_2O_5 (3 mol) for 30 minutes to 1 hour with ethanol. An excess of K_2CO_3 was needed to accommodate vaporization. The mixture was dried at 60° C for 3-4 hrs and then calcinated for 15 min at 1473 K, with a ramp rate of 20 K/min. Resulting crystals were colorless and flaky, resembling mica. The crystals were removed from the crucible with water and a glass rod, water was removed by centrifuge and decanting, and the crystals were ground with ethanol by mortar and pestle for another 30 minutes to 1 hour.[36] These were dried at 60° C overnight and their structure was confirmed by X-Ray Diffraction Spectroscopy (XRD).[37]

To produce hexaniobate scrolls, $K_4Nb_6O_{17}$ was acid-exchanged with 0.25 M H_2SO_4, with shaking, for 24 hrs. The material was then rinsed several times with water, by centrifuging and decanting, until the pH of the rinse returned to neutral. The protonated sheets were exfoliated by shaking with 8 wt. % TBAOH (125 mL) for 24 hours. Exfoliated scrolls were separated from the non-exfoliated sheets by centrifuge so that the plates settled to the bottom while the scrolls remained suspended and could be poured off. The scrolls were collected by adding concentrated HCl to the suspension until they crashed out. The rinsing procedure applied after exfoliation was repeated to return the scrolls to a neutral pH and they were dried by baking at 60° C overnight.[36] Composition of the product was again confirmed by XRD.[35,38]

Platinum nanoparticles were photodeposited onto 30 to 50 mg batches of scrolls at a time. The scrolls were sonicated for approximately 2 minutes in 9 mL water to suspend them before adding 1 mL HPLC grade methanol and the required amount of 1.315 wt % of $H_2PtCl_{6(aq)}$ for the desired weight percent of Pt. The suspension was purged with Ar in the dark, with stirring, for the length of the photodeposition. The suspension was irradiated with a 300 W Xe/HgXe arclamp for 2 hours, with continued purging and stirring. Before the photodeposition, the suspension was faintly grey in color, but darker afterwards. Platinized scrolls were collected and rinsed with DI water as before to remove remaining H_2PtCl_6, and baked overnight at 60° C to dry.[36]

$Ru(bpy)_2(4,4'\text{-}(PO_3H_2)_2bpy)^{2+}$ dye (abbreviated RuP^{2+}) was adsorbed the day before the photolysis experiments in 7.5 g batches of scrolls. Maximum hydrogen evolution was found by Maeda to occur with 12 μmol dye per 1 g scrolls, so 0.09 μmol dye was used for each batch. The scrolls were sonicated briefly in 2 mL aqueous solution of 6 mM dye and the suspension was stirred in the dark for 1 hr. The dye-adsorbed-scrolls were collected and rinsed by centrufigation and the supernatant was reserved and analyzed by UV-VIS spectrometer. The amount of dye adsorbed was determined by difference in absorbance between the initial dye solution and the supernatant. Scrolls were again dried by a 60° C overnight bake.[7]

3.3. Time-Resolved Photolysis Procedures

Before beginning flash photolysis studies, it was necessary to reproduce the time-resolved studies that had already been done by Dr. Maeda, as a means of testing the

quality of the synthesized system. In time-resolved photolysis, the sample is sealed and purged with an inert gas, in this case Ar. The sample is irradiated with a known wavelength of light; a 300 W Xe/HgXe arclamp fitted with a 450 nm bandpass filter was used for these experiments. Periodically, a sample of gas is drawn from the headspace of the vial and injected into a GC in order to determine the amount of hydrogen (and oxygen and nitrogen) in the vial.[36] The amount of hydrogen, of course, indicated the quantum yield of the system (4). Any change in the amount of nitrogen present in the system would be indicative of a leak, whereas any decrease in the amount of oxygen, relative to the nitrogen, suggests a significant back reaction, where the system may be catalyzing the recombination of oxygen and hydrogen to form water.

Max available current	$I_{hv} = P_c/V$	(4)
Power to the cell	$P_c = (P_m/A_m)A_c$	
Energy (voltage) per electron	$V = (\hbar c/\lambda)(1\ eV/1.602E\text{-}19\ J)$	
Current resulting in H_2	$I_H = (H2\ molecules/s)(1\ e\text{-}/H2)$	
Quantum Yield	$QY = (I_H/I_{hv})(100\%)$	

In the above equations, P_m is the lamp power measured by the power meter, A_m is the area measured by the power meter (which was covered by the beam spot), and A_v is illuminated area of the reaction vessel. Only one electron is needed for the reduction of H^+ to H_2 because of current doubling, whereby the oxidized EDTA radical injects a second electron directly into the semiconductor in addition to the regularly assumed pathways.[7]

Time-resolved photolysis experiments were carried out as follows. A 5.0 mg sample of nanoscrolls was suspended in 2 mL (10 mM) $EDTA{\cdot}Na_{2(aq)}$, pH 4.5, unbuffered. For those experiments involving the electrostatically attracted $Ru(bpy)_3^{2+}$ dye rather than the chemisorbed phosphonated version, this solution included 50 mM $Ru(bpy)_3Cl_2$. The reaction vessel was an 11.0 mL pyrex vial with squared walls which was sealed with a rubber septum and enclosed by an outer glass jacket. Argon flowed continuously through the outer jacket. The reaction vessel was purged for 10-15 min, or however long it took to remove the oxygen and nitrogen peaks from the sample headspace, when tested by GC. The sample was irradiated with a 300 W Xe/HgXe lamp which was fitted with a 450 bandpass filter and warmed up for a minimum of 15 minutes before beginning photolysis.[36]

To ensure the correct use of the time-resolved photolysis system, I first measured the hydrogen evolution of some samples that had been previously synthesized and measured by Dr. Maeda. For a platinized titania sample, I measured a quantum yield of 0.66%, in comparison to the 1% yield that Dr. Maeda measured. For a platinized calcium niobate $HCa_2Nb_3O_{10}$ sample, I measured a quantum yield of 9.1%, vs. Dr. Maeda's 10%.[7] I did not adsorb the amount of dye recommended for maximum quantum yield on this sample, because by using 8 μmol/g sample instead of 12 μmol/g sample, Dr. Maeda lost only 1 μmol/hr of hydrogen, and I wished to conserve the dye. I decided that this quantum yield therefore demonstrated appropriate use of the photolysis system (Fig. 14).

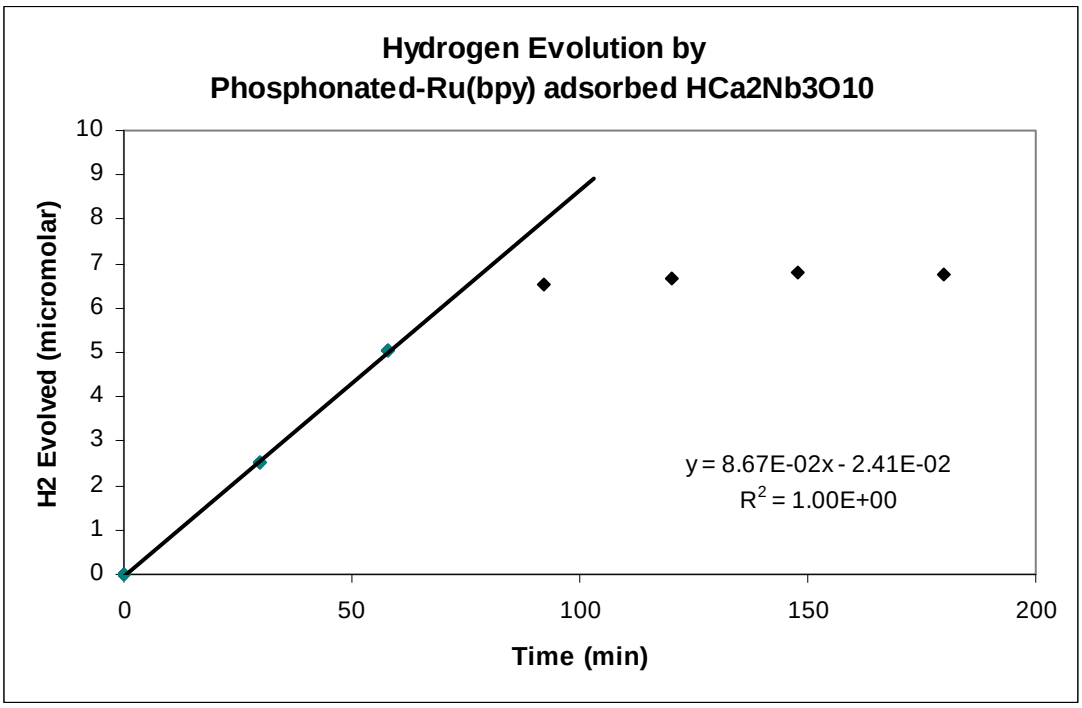

Figure 14: Hydrogen evolution using an $HCa_2Nb_3O_{10}$ sample prepared by Kazuhiko Maeda to check photolysis technique

3.4. Troubleshooting Low Quantum Yields

3.4.1. Ageing of the Platinum Catalyst

The quantum yield found for my nanoscroll system was only 1.8%, whereas Dr. Maeda found a quantum yield of 10% with his fabrication. The platinized sample which was imaged and which had been used in photolysis was used approximately two weeks after photodeposition. As photolysis had, in the past, been run only a day or two after

deposition, it seemed likely that the low quantum yields were due to degraded catalysts. Photolysis experiments were repeated with freshly platinized scrolls and the quantum yield of the same batch of scrolls was measured again after approximately two weeks. For one batch of scrolls, the quantum yields were higher immediately after the photodeposition (3.3% fresh vs. 1.6% old), but with the other batch of scrolls, the quantum yields were approximately equal (1.5% fresh vs. 1.8% old).

3.4.2. Low Platenization Yields

TEM images were taken of the plain and platinized nanoscrolls in order to compare them with Dr. Maeda's (Fig. 15). Although some Pt nanoparticles can be seen on the surface of the platinized scrolls, there are far fewer than were seen in images in Dr. Maeda's published work, suggesting that the cause of the low quantum yields may have been the relative deficiency of platinum nanoparticles.[36] Earlier attempts had followed the results of Dr. Maeda's 2008 paper, which had found highest quantum yields with 0.3 wt. % Pt per scroll for a $Ru(bpy)_3^{2+}$ sensitizer.[36] A later paper found higher yields with 0.5 wt. % Pt per scroll while using a phosphonated ruthenium polypyridyl sensitizer.[7] Scrolls were therefore prepared using the higher recommended weight percentage of platinum and the chemisorbed phosphonated dye. Average quantum yields were slightly higher (2.5%) than they had been for previous samples (1.5%) but still far lower than the expected 10%. TEM images of the higher weight percentage particles did not reveal more Pt deposits.

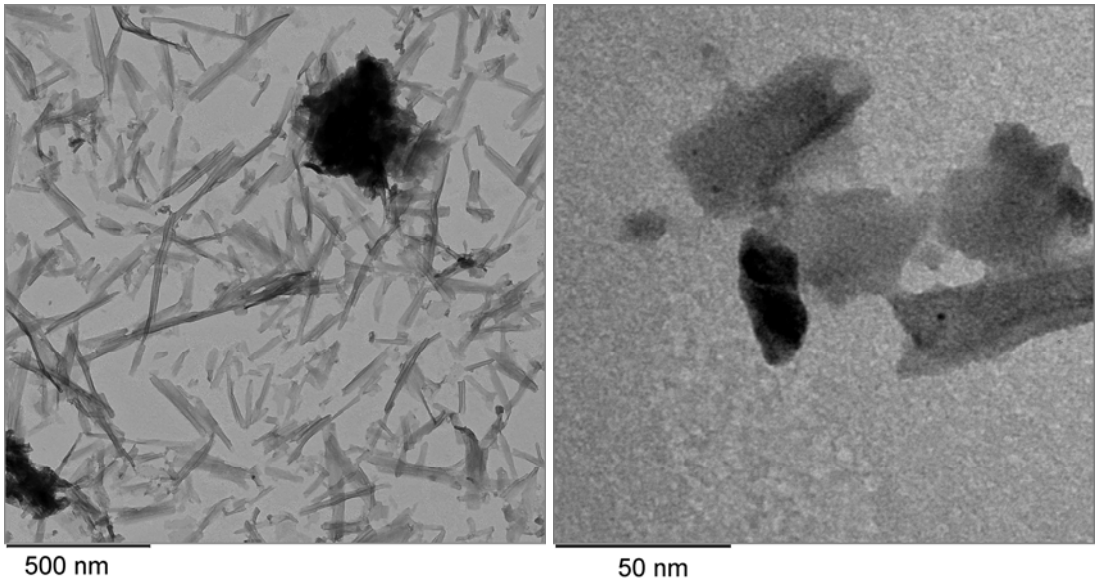

Figure 15: TEM images of $H_4Nb_6O_{17}$ nanoscrolls; unplatinized (left) and platinized (right).

It was found that the lamp intensity measured with photolysis at this time was much lower than in previous experiments, averaging 3.6 mW as opposed to 7 mW for Dr. Kazu's experiments, possibly resulting in less photodeposition under the same conditions. Another 300 W Xe/HgXe lamp with a much higher intensity was used for the photodepositions, but quantum yields increased only marginally, from 1.3% to an average of 2.7%. The intensity of the lamp used in the actual photolysis experiment should not affect the quantum yield, since the intensity of the 450 nm bandpass-filtered lamp is measured with a light meter at the time of photolysis and factored into the quantum yield calculations. The lamp intensity may, however, have affected the total hydrogen evolved in a given photolysis experiment. Unfortunately, the higher intensity lamp in our lab was not close enough to the GC to allow for its use in the photolysis experiments.

Post-deposition samples of scrolls did not show the expected homogeneity in coloration. The majority of the sample was a very light grey, but a small portion of the sample which was the last to settle out of suspension during centrifugation was a much darker grey. If a substantial amount of the platinum in solution was depositing onto something other than the nanoscrolls, this would explain both the low quantum yields and the relative absence of Pt shown by TEM. It was considered that the platinum may be depositing onto the Teflon stir-bar, but this hypothesis was disproved when substitution of a glass magnetic stir-bar during platinization yielded approximately the same

proportion of darker material. It was then considered that the platinum may be depositing onto the glass wall of the scint vial during deposition and peeling off, as this had been observed by another researcher during a different platinization procedure in our lab. In an attempt to avoid this, the positioning of the reaction vessel (scint vial) during deposition was altered so that the beam path traveled through the glass-solution interface as little as possible, traveling through the glass-air and air-solution interfaces instead. This deposition setup produced similar amounts of the darker material and quantum yields of 2.9%, in comparison with 3.3% and 2.0% quantum yields for irradiation through the glass-solution interface.

3.4.3. Differences in Surface Areas

The surface area of Dr. Maeda's scrolls was not known, but it seemed possible that the different grinding techniques might result in a difference in the surface area, which would alter the ideal platinum loading weight percentages. Because of the relative lack of platinum particles shown by TEM and because of the similarity in quantum yield between 0.5 and 0.3 wt % scrolls, a higher weight percentage was tried first. It was also considered that using more platinum might compensate if some was indeed depositing onto something other than the scrolls. A batch of scrolls was therefore prepared with 0.7 wt % Pt, which produced a quantum yield of 1.8%, vs. the average 2.7% found with 0.5 wt % Pt scrolls. This line of inquiry was interrupted by another more promising one.

3.5. Troubleshooting Early Reaction Endpoints

Upon reviewing some of the photolysis data, it was found that the quantum yields were not the only aspect that was unexpected. In past work, it had been found that the amount of sacrificial donor (in this case, EDTA) determined the end point of the reaction.[7] My photolysis experiments were producing far less hydrogen than was expected for the calculated amount of EDTA in solution. Although photolysis with a fresh batch of EDTA appeared to improve the total hydrogen evolution of the system from an average of 4.8 μmol to 8.1 μmol, this data is inconclusive as the 4.8 mol average includes an outlier of 13.0 μmol. The fresh solution of EDTA did nothing to improve the quantum yield. Upon closer review of my past experiments, it was found that the total hydrogen evolved in each experiment was inconsistent even from one run to the next.

This seemed indicative of a systematic error, so the GC was tested for repeatability and recalibrated for hydrogen, oxygen, and nitrogen.

When the GC was found to give repeatable data and the new calibration curves did not significantly alter the quantum yield or the total evolved hydrogen, the system was tested for leaks. Monitoring of oxygen and nitrogen peak areas during the course of a past photolysis experiment had shown no significant leak between the reaction vessel and the room atmosphere (i.e. a large increase in nitrogen with time), regardless of whether the EDTA was reacting with molecular oxygen (i.e. a decrease in the oxygen/nitrogen ratio) (Fig 16). In order to test the possibility of a leak between the reaction vessel headspace and the surrounding jacket, nitrogen was flowed through the outer jacket instead of argon, so as to register on the GC, and the vial was purged with hydrogen. This did demonstrate a significant leak, which was notably reduced by replacement of the old septum with a new one. It also confirmed the absence of a leak between the vessel and the room, since no oxygen was detected for the length of the run (Fig 17).

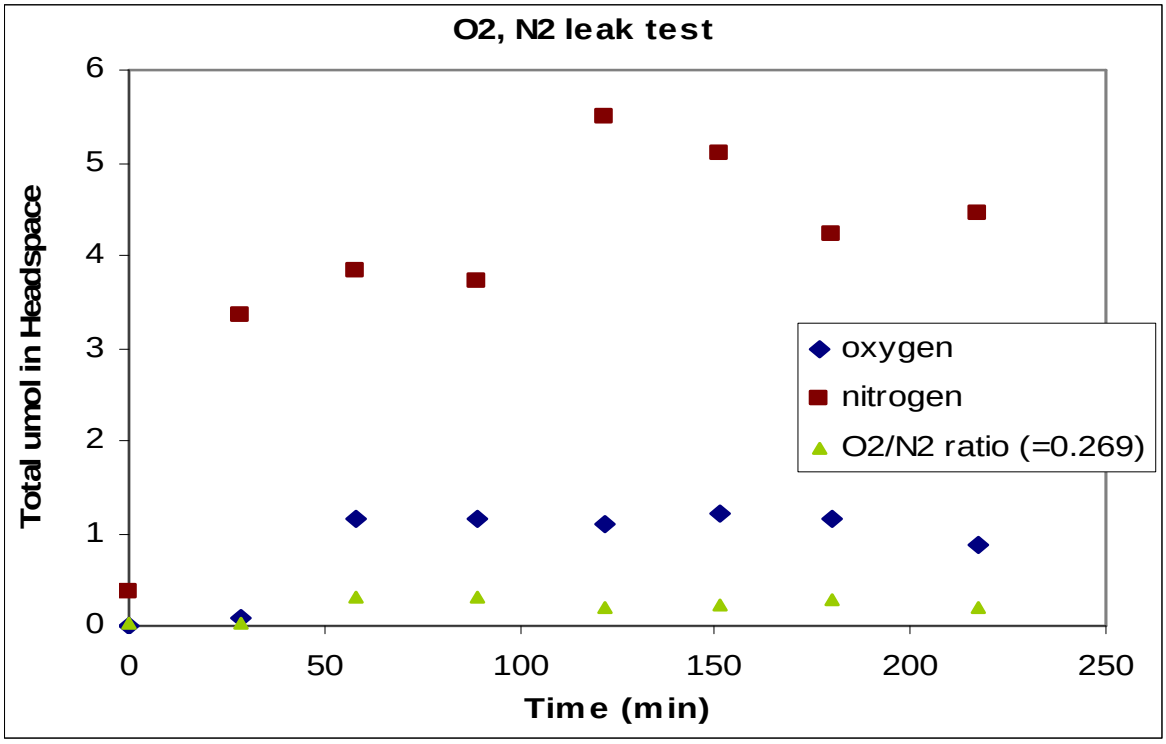

Figure 16: Change in Oxygen and Nitrogen levels during a photolysis experiment

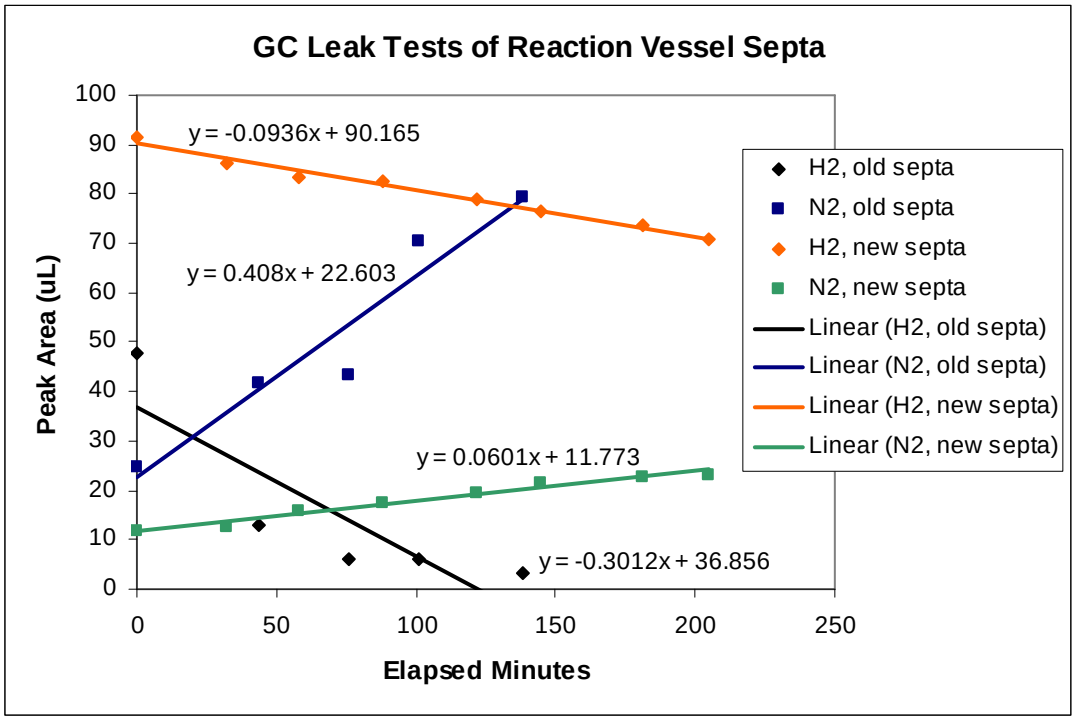

Figure 17: Hydrogen leak into Ar-purged jacked with old and new septa

With the new GC calibration curves and the new reaction vessel septum minimizing the leak, the photolysis experiment was repeated, taking great care to avoid any of the potential problems mentioned above. That photolysis resulted in by far the largest total hydrogen evolution, at 13 μmol, but only 2.9% quantum yield (Fig. 18). The quantities of nitrogen and oxygen found in the headspace did not match with any data (Fig 19).

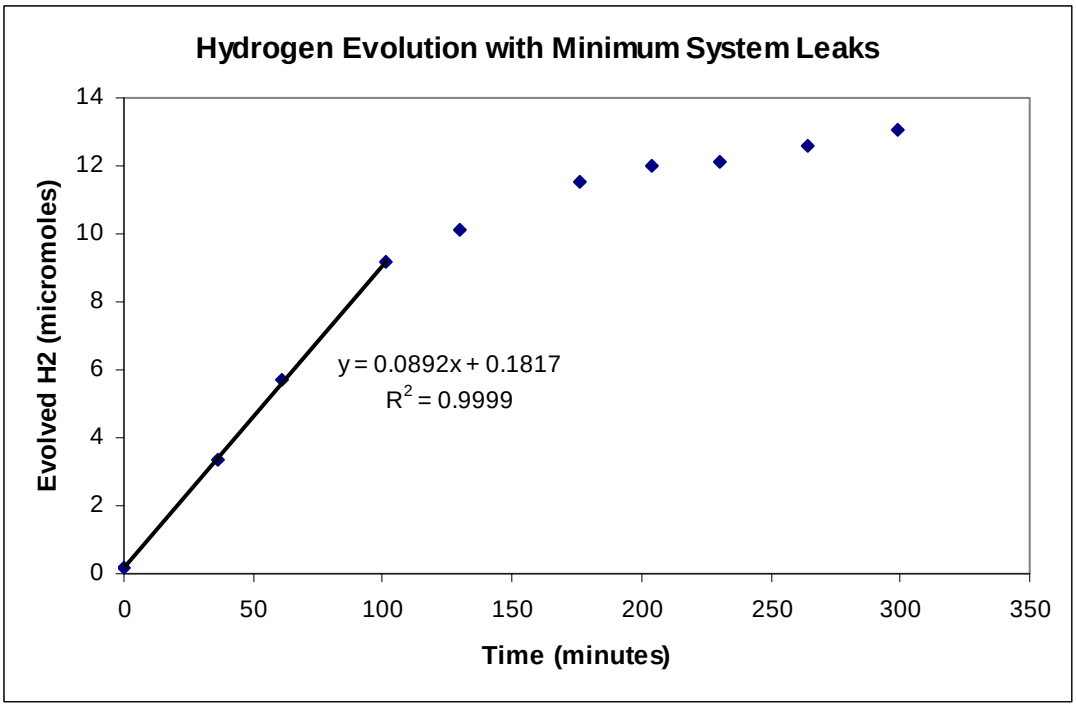

Figure 18: Photolysis on platinized hexaniobate ($H_4Nb_6O_{17}$) nanoscrolls with adsorbed RuP^{2+} dye for a total hydrogen evolution of 13.0 umol and a quantum yield of 2.9%

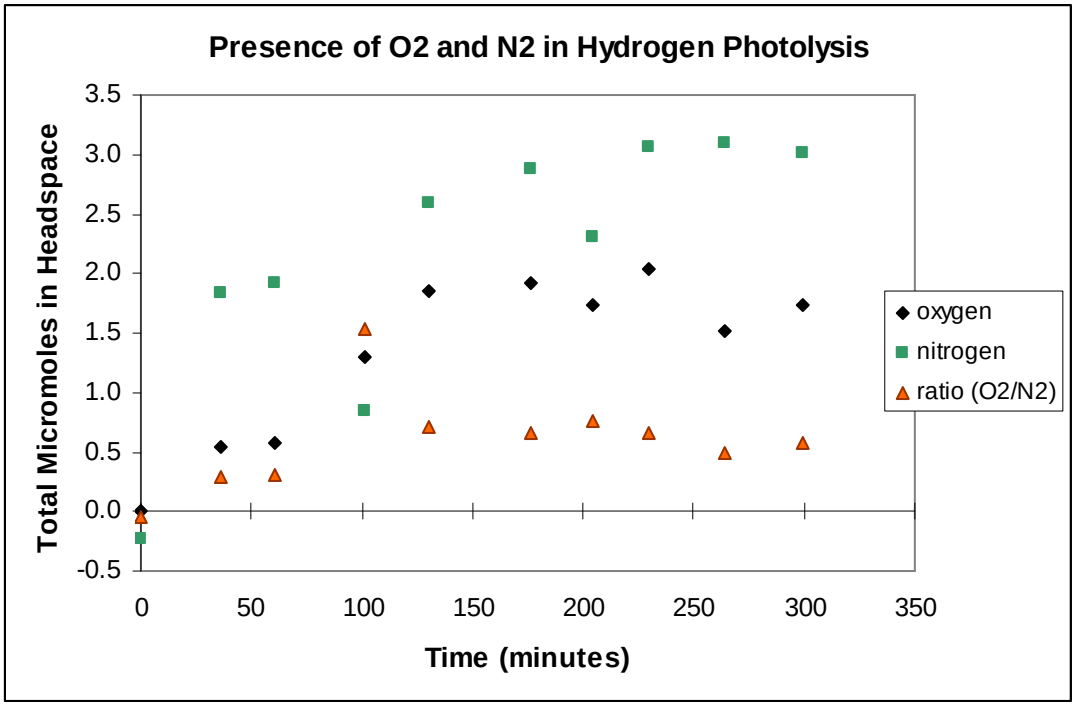

Figure 19: Nitrogen and Oxygen presence in photolysis experiment shown in Fig. 18

At this point in time, it was decided that a more time-efficient way to improve the quantum yield of the system would be to measure the electron-transfer rates by way of transient photolysis. This direction of study was therefore halted in favor of assembling and testing a system of diffuse reflectance spectroscopy.

References

1. Bolton, J. Solar Photoproduction of Hydrogen: A Review. *Solar Energy*, **1996**, *57*, 37.
2. (a) Chen, D; Ye, J. Selective-synthesis of high-performance single-crystalline Sr2Nb2O7 nanoribbon and SrNn2O6 nanorod photocatalysts. *Chem. Mater*. **2009**, *21*(11), 2327-2333. (b) Kudo, A; Miseki, Y. Heterogeneous photocatalyst materials for water splitting. *Chem. Soc. Rev*. **2009**, *38*, 253-278. (c)Maeda, K.; Teramura, K.; Takata, T.; Hara, M.; Saito, N.; Toda, K.; Inoue, Y.; Kobayashi, H.; Domen, K. Overall water splitting on (Ga1-xZnx)(N1-xOx) solid solution photocatalyst: Relationship between physical properties and photocatalytic activity. *J. Phys. Chem. B* **2005**, *109*, 20504-20510.
3. Bolton, J.; Strickler, S.; Connolly, J. Limiting and realizable efficiencies of solar photolysis of water. *Nature*. **1985**, *316*, 495.
4. Harriman, A.; Pickering, I; Thomas, J; Christensen, P. Metal Oxides as Heterogeneous Catalysts for Oxygen Evolution under Photochemical Conditions. *J. Chem. Soc., Faraday Trans. 1*, **1988**, *84*(8), 2795.
5. Hoertz, P.; Kim, Y.; Youngblood, W. J.; Mallouk, T. Bidentate Dicarboxylate Capping Groups and Photosensitizers Control the Size of IrO2 Nanoparticle Catalysts for Water Oxidation. *J. Phys. Chem B* **2007**, **111**, 6845.
6. Youngblood, W.J.; Lee, S.-H. A.; Kobayashi, Y.; Hernandez-Pagan, E.A.; Hoertz, P.; Moore, T.A.; Moore, A.L.; Gust, D; Mallouk, T.E. *J. Am. Chem. Soc.* **2009**, *131*(3), 926-927.
7. Maeda, K.; Eguchi, M.; Lee, S.A.; Youngblood, W.J.; Hata, H.; Mallouk, T.E. Photocatalytic Hydrogen Evolution from Hexaniobate Nanoscrolls and Calcium Niobate Nanosheets Sensitized by Ruthenium(II) Bipyridyl Complexes. *J. Phys. Chem. C* **2009**, *113*, 7962-7969.
8. Goldsmith, J. I.; Hudson, W. R.; Lowry, M. S.; Anderson, T. H.; Bernhard, S.; *J. Am. Chem. Soc.* **2005**, *127*, 7502-7510.
9. Harriman, A.; Richoux, M.; Christensen, P.A.; Moseri, S.; Neta, P. *J.Chem. Soc., Faraday Transactions I* **1987**, *83*, 3001.
10. Maeda, K.; Teramura, K.; Lu, D; Takata, T.; Saito, N.; Inoue, Y.; Domen, K. Characterization of Rh-Cr Mixed-Oxide Nanoparticles Dispersed on (Ga1-xZnx)(N1-xOx) as a Cocatalyst for Visible-Light-Driven Overall Water Splitting. *J. Phys. Chem. B* **2006**, *110*, 13753.
11. Sakamoto, N.; Ohtsuka, H.; Maeda, K.; Lu, D.; Kanehara, M.; Teramura, K.; Teranishi, T.; Domen, K. Highly Dispersed Noble Metal Nanoparticles with Cr2O3 Shell as Efficient Hydrogen Evolution Sites for Photocatalytic Overall Water Splitting. *Angew. Chem. Int. Ed*. Paper pending.
12. Maeda, K.; Teramura, K.; Lu, D.; Saito, N.; Inoue, Y.; Domen, K. Noble-Metal/Cr2O3 Core/Shell Nanoparticles as a Cocatalyst for Photocatalytic Overall Water Splitting. *Angew. Chem. Int. Ed.* **2006**, *45*, 7806.
13. Trasatti, S. Electrocatalysis of Hydrogen Evolution: Progress in Cathode Activation. In *Advances in Electrochemical Science and Engineering*; Gerischer, H.; Tobias, C. W., Eds.; VCH: Weinheim, 1990, Vol. 2, pp 48.
14. Hata, H.; Kobayashi, Y.; Bojan, W.; Youngblood, W.J.; Mallouk, T.E. Direct

deposition of trivalent rhodium hydroxide nanoparticles onto a semiconducting layered calcium niobate for photocatalytic hydrogen evolution. *Nano Letters,* **2008**, *8*(3), 794-799.
15. Yan, Y.; Li, Q.; Huo, S.; Ma, M.; Cai, W.; Osawa, M. Ubiquitous Strategy for Probing ATR Surface-Enhanced Infrared Absorption at Platinum Group Metal-Electrolyte Interfaces. *J. Phys. Chem. B* **2005**, *109*, 7900.
16. Zou, S.; Weaver, M. Surface-Enhanced Raman Scattering on Uniform Transition-Metal Films: Toward a Versatile Adsorbate Vibrational Strategy for Solid-Nonvacuum Interfaces? *Anal. Chem.* **1998**, *70*, 2387.
17. Gorer, S.; Lui, H.; Stiger, R.; Zach, M.; Zoval, J.; Penner, R. Electrodeposition of Metal Nanoparticles on Graphite and Silicon. In *Metal Nanoparticles; Synthesis, Characterization, and Applications*; Feldheim, D.; Foss, C., Eds.; Marcel Dekker, Inc.: New York, 2002.
18. Bard, A. J.; Faulkner, L. R. Electrochemical Methods: Fundamentals and Applications. John Wiley & Sons, Inc.: USA, 2001, pp 340-344, 609-619.
19. Maeda, K.; Teramura, K.; Lu, D.L.; Saito, N; Inoue, Y.; Domen, K. Roles of Rh/Cr2O3 (core/shell) nanoparticles photodeposited on visible-light-responsive (Ga1-xZnx)(N1-xOx) solid solutions in photocatalytic overall water splitting. *J. Phys. Chem. A.* **2007**, *111*, 7554-7560.
20. Zhdanov, S.I. Sulfur. In *Encyclopedia of Electrochemistry of the Elements*; Bard, A.J., Ed.; PUBLISHER: PLACE, DATE, Vol. 4, pp 341.
21. Swathirajan J.; Bruckenstein, S. *Electroanal. Chem.,* **1984**, *163*, 77-92.
22. Albery. *Proc. Chem. Soc.* **1963**, *169*, PAGES
23. Swathirajan; Bruckenstein. *Z. Phys. Chem. Neue Folge* **1983**, *136*, 197.
24. Swathirajan; Bruckenstein. *Z. Phys. Chem. Neue Folge* **1983**, *136*, 215.
25. Pourbaix, M. Atlas of electrochemical equilibria in aqueous solutions. Pergamon Press: New York, NY, 1966.
26. Leuthold, A.C.; Wakai, R.T. U.S. Patent 5592732, 1997.
27. Mikhailova, L.A.; Kasatkin, E.V.; Kasatkin, V.E.; and Prutchenko, S.G. *Russian Journal of Electrochemistry*, **2000**, *36*(8), 866-873.
28. Vaskevich, A.; Posenblum, M.; and Gileadi, E. *J. Electrochem. Soc.,* **1995**, *142*(5), 1502-1508.
29. Woods, R. Chemisorption at Electrodes. In *Electroanalytical Chemistry*; Bard, A.J., Ed.; M. Dekker Inc: PLACE, 1976, Vol. 9, PAGES
30. Carvalhal, R.F.; Freire, R.S.; Kubota, L.T. *Electroanalysis,* **2005**, *17*(14), 1251-1259.
31. Yang, W.; Hernandez, R.M.; Bartlett, D.J., Jr.; Bingham, J.M.; Kline, T.R.; Sen, A.; Mallouk, T.E. *Langmuir* **2006**, *22*, 10451-10456.
32. Cannes, C.; Kanoufi, F.; Bard, A.J. *Journal of the Electrochemical Society* **2003**, *547*, 83-91.
33. Kim, Y.I.; Salim, S.; Juq, M.J.; Mallouk, T.E. Visible Light Photolysis of Hydrogen Iodide Using Sensitized Layered Semiconductor Particles. *J. Am. Chem. Soc.* **1991**, *113*, 9561-9563.
34. Kim, Y.I.; Atherton, S.J.; Brigham, E.S.; Mallouk, T.E. Sensitized Layered Metal Oxide Semiconductor Particles for Photochemical Hydrogen Evolution from Nonsacrifical Electron Donors. *J. Phys. Chem.* **1993**, *97*, 11802-11810.

35. Suape, G.B.; Mallouk, T.E.; Won, K.; Schmehl, R.H. Visible Light Photolysis of Hydrogen Iodide Using Sensitized Layered Metal Oxide Semiconductors: The Role of Surface Chemical Modification in Copntrolling Back Electron Transfer Reactions. *J. Phys. Chem B* **1997**, *101*, 2508-2513.
36. Maeda, K.; Eguchi, M.; Youngblood, W.Y.; Mallouk, T.E. Niobium Oxide Nanoscrolls as Building Blocks for Dye-Sensitized Hydrogen Production from Water under Visible Light Irradiation. *Chem. Mater.* **2008**, *20*, 6770-6778.
37. K. Nassau, J. W. Shiever, and J. L. Bernstein, J. Electrochem. Soc. 1969, 116, 348 Saupe, G.B.; Waraksa, C.C.; Kim H.-N.; Han, Y.J.; Kaschak, D.M.; Skinner, D.M., Mallouk, T.E. Nanoscale tubules formed by exfoliation of potassium hexaniobate. *Chem. Mater.* **2000**, *12*, 1556-1562.
38. Kobayashi, Y.; Hata, H.; Salama, M.; Mallouk, T.E. Scrolled Sheet Precursor Route to Niobium and Tantalum Oxide Nanotubes. *Nano Lett,* **2007**, *7*, 2142-2145.